Microelectronics Reliability 93 (2019) 61–71

Contents lists available at ScienceDirect

Microelectronics Reliability

journal homepage: www.elsevier.com/locate/microrel

Effect of PCB cracks on thermal cycling reliability of passive microelectronic components with single-grained solder joints

Saeed Akbari*, Andreas Lövberg, Per-Erik Tegehall, Klas Brinkfeldt, Dag Andersson

RISE Research Institutes of Sweden, Box 104, SE-431 22 Mölndal, Sweden

ARTICLE INFO

Keywords:
Lead-free soldering
PCB cracking
Anisotropy of tin grains
Passive components
Finite element modelling

ABSTRACT

Lead-free tin-based solder joints often have a single-grained structure with random orientation and highly anisotropic properties. These alloys are typically stiffer than lead-based solders, hence transfer more stress to printed circuit boards (PCBs) during thermal cycling. This may lead to cracking of the PCB laminate close to the solder joints, which could increase the PCB flexibility, alleviate strain on the solder joints, and thereby enhance the solder fatigue life. If this happens during accelerated thermal cycling it may result in overestimating the lifetime of solder joints in field conditions. In this study, the grain structure of SAC305 solder joints connecting ceramic resistors to PCBs was studied using polarized light microscopy and was found to be mostly single-grained. After thermal cycling, cracks were observed in the PCB under the solder joints. These cracks were likely formed at the early stages of thermal cycling prior to damage initiation in the solder. A finite element model incorporating temperature-dependant anisotropic thermal and mechanical properties of single-grained solder joints is developed to study these observations in detail. The model is able to predict the location of damage initiation in the PCB and the solder joints of ceramic resistors with reasonable accuracy. It also shows that the PCB cracks of even very small lengths may significantly reduce accumulated creep strain and creep work in the solder joints. The proposed model is also able to evaluate the influence of solder anisotropy on damage evolution in the neighbouring (opposite) solder joints of a ceramic resistor.

1. Introduction

Thermo-mechanical fatigue of solder joints arising from mismatch in material properties between component, solder, and printed circuit board (PCB) is a major reliability issue in microelectronics assemblies [1–5]. Fatigue life of solder joints is often studied using accelerated thermal cycling tests which employ higher temperature ranges and faster ramp rates than those found in field conditions [6–8]. Also, finite element simulations can complement the experimental observations by providing more insights into mechanisms governing damage initiation and propagation in solder joints [9–11].

Grain morphology of lead-free solder alloys significantly affects damage evolution and failure under thermal cycling and needs to be investigated thoroughly to enhance the accuracy of solder joints' life prediction models. Previous studies on solidification in different tin-based solder joints have shown that they are mostly single-grained [12,13]. It has also been shown that the grains have nearly random orientation [14–16]. The randomness of the grain orientations of adjacent joints cause each solder joint to undergo a unique stress and strain state. Numerous studies have shown that for a ball grid array (BGA) component, the joint with the maximum damage which fails first is not necessarily located at the position of the highest strain due to the global CTE mismatch (normally the point with the maximum distance from the neutral point or under the edge of the chip) [12,13,17]. This is a consequence of random orientation of the grains in single-grained solder joints with highly orientation-dependant, i.e. anisotropic, properties that generates stresses and strain states varying among neighbouring joints.

In addition, the transition to lead-free solder alloys has increased the risk of cracking of plated through-holes (PTHs) during soldering, because the reflow temperature of lead-free alloys is higher than leaded solders [18]. This raises the thermal-mechanical stresses induced in the reflow process on the PTHs. Therefore, PCB laminates with high glass transition temperature (T_g) and low coefficient of thermal expansion (CTE) have been developed to withstand lead-free soldering and to generate low stress on the PTHs [19]. The high T_g and low CTE are achieved by using a resin with a high degree of cross-linking and a high content of inorganic fillers. This results in a laminate with a high elastic modulus but also a laminate that is more brittle than traditional low T_g laminates [20,21]. The higher elastic modulus of laminates will result

* Corresponding author.
E-mail address: saeed.akbari@ri.se (S. Akbari).

https://doi.org/10.1016/j.microrel.2019.01.006
Received 26 October 2018; Received in revised form 21 December 2018; Accepted 5 January 2019

in higher stress levels both in the solder joints and in the PCB laminate during thermal cycling. In addition, since lead-free solders are stiffer than leaded solders, they apply more stresses to the PCB.

The highest thermo-mechanical stress that solder joints will be exposed to will occur during the cooling phase after soldering. Hence, PCB cracks may form early in the soldering process. Even very small cracks in the PCB initiated during soldering can change the dominant failure mode from fatigue cracking of the solder joints to PCB cracking [22]. In fact, it has been shown that pre-stress on PCB prior to a thermal cycling test may cause latent damages in the PCB which cannot be observed as cracks in cross-sections, but nevertheless increase the risk for PCB cracking in a subsequent thermal cycling test [23].

A PCB provides the mechanical support and electrical connection for various electronic components assembled on it. It is typically a laminated polymeric composite consisting of an epoxy resin matrix bonding woven bundles of glass fibres. Similar to other laminated composites the mechanical properties of a PCB are highly anisotropic. The in-plane stiffness and tensile strength of PCBs are much larger than the out-of-plane stiffness and tensile strength. In other words, PCBs are much stronger in fibre direction than in the transverse direction (normal to the PCB). It has been shown that the transverse tensile strength is usually of the same order of magnitude as that of the epoxy resin bonding the glass fibres [24].

The fatigue life of solder joints is predicted from accelerated thermal cycling test results by using acceleration factors to extrapolate life in field conditions. This is based on the assumption that the failure mechanisms in both test and field conditions are similar. This assumption may be wrong, since PCB cracking is more likely to occur under test conditions because thermal cycling parameters used in tests are normally harsher than those found under typical field conditions. Therefore, the partial inconsistency of the failure mechanisms and the role of PCB cracking to reduce strain in solder joints may result in an overestimation of solder fatigue life obtained from accelerated testing [13,25].

PCB cracking has already been reported for lead-free BGA packages. Tegehall and Wetter [13] detected PCB cracking for three types of BGA packages assembled on a 1.6 mm thick PCB with SAC305 solder joints, which were subsequently thermally cycled between −40 °C and +125 °C. It was shown that the formation of the cracks in the PCB beneath the solder joints improves the thermal fatigue life of the solder joints by increasing the PCB compliance and lowering the stress and strain in the solder joints. Hagberg et al. [26] also reported that the BGA solder joints close to the PCB cracks were less damaged, confirming that PCB cracking is a crucial parameter in thermal cycling reliability of BGA packages.

While research on thermal cycling reliability of single-grained solder joints has been mostly focused on area array components, the present study investigates this effect for ceramic resistors. Polarized light microscopy is used to study the grain structure of SAC305 solder joints connecting ceramic resistors to PCBs, and UV light is used to detect cracks in the PCB laminate. To explain the experimental observations of PCB cracking and solder failure, a finite element model is developed to study the effect of random orientation of the two opposite solder joints of a ceramic resistor on the formation of cracks in the PCB, and the subsequent effect of PCB cracking on damage evolution in solder joints under thermal cycling. Accumulated creep strain and creep work are the two parameters used to quantify damage evolution in the solder joints. It is shown that the damage reduction in solder joints due to PCB cracking is proportional to the crack length.

2. Tin anisotropic properties

Most lead-free solder alloys used in electronics contain at least 95% tin to facilitate soldering at temperatures tolerable to various parts of electronic assemblies [14]. When solidifying in the soldering process, the tin forms β-Sn. As shown in Fig. 1, β-Sn properties are highly orientation and temperature dependant. Interestingly, both elastic modulus and CTE are greatest in [001] direction (along the *c*-axis). The CTE in [100] and [010] directions (along the *a*-axis and *b*-axis) is about half of that in the [001] direction [27]. This ratio remains constant for different temperatures. Although the CTE peanut-shaped distribution uniformly expands in all directions from −45 °C to 135 °C, the elastic modulus distribution becomes more anisotropic with temperature increase. The elastic modulus along the *c*-axis is almost three times larger than that along *a*- and *b*-axes at −45 °C. This ratio constantly increases with temperature.

After solidification, lead-free solder joints can take three different grain structures: single grained (SG), cyclic twinned grained (CTG), and interlaced twinned grained (ITG) structure. An individual joint can also have a mixture of CTG and ITG structures. The grain structure depends on various manufacturing parameters such as joint size, surface finish on soldered surfaces, and cooling rate during soldering [28]. Previous studies have shown that lead-free solder joints to BGAs are often single-grained [13,25,29–31], because these joints usually undercool 20–80 °C and solidify in a single nucleation event. Moreover, since the single-grained solder joints are highly anisotropic, their orientation significantly affects the solder stress and strain distribution under different thermal and mechanical loadings [13].

Following the colour scale proposed in [12] and assuming random grain orientation, the probabilities of various *c*-axis orientations (from 0° to 90°) are depicted in Fig. 2 with five different colours. Each colour shows an interval of 18°. On the two extremes, there exist red and blue joints. A joint with *c*-axis almost parallel to the board is referred to as a red joint, while a joint with *c*-axis almost perpendicular to the board is referred to as a blue joint. Fig. 2 indicates that the probability of a red joint is about six times higher than a blue joint.

In surface mount microelectronic assemblies with multi-joint configurations such as resistors and BGAs, interaction of neighbouring single-grained solder joints with different orientations produces stress and strain states unique to each joint and complicates lifetime predictions. Stress and strain levels during temperature changes depend on the relative mismatch in thermomechanical properties between component, solder, and board, which is a function of the orientation of the single-grained solder joints. For instance, since the CTE of the PCB parallel to the board is about 15 ppm, for a single-grained solder joint the local mismatch in the CTE between the solder joint and the board is maximum when the *c*-axis is parallel to the board (red joint), and minimum when the *c*-axis is perpendicular to the board (blue joint).

The alternating tensile and compressive stresses and strains in single-grained solder joints during thermal cycling could influence the stress and strain state in component and PCB laminate. Therefore, random orientation of single-grained solder joints is a key parameter in damage initiation and propagation both in the component and in the board. Finite element analysis is a strong tool that enables detailed study of various parameters affecting solder damage, and prediction of the locations of damage initiation in the component and the PCB.

3. Experimental method

Zero-ohm ceramic resistors 1206 (CR1206) were soldered to a six-layers 1.6 mm thick FR4 PCB using SAC305 alloy (Sn with 3.0% Ag and 0.5% Cu). Fifty soldered resistors were split into ten test patterns. Each pattern consisted of five resistors connected in series. The dimensions of the solder lands were 2.0 × 1.1 mm and the distance between the solder lands was 1.9 mm. The thickness of the stencil used for printing solder paste on the solder lands was 0.127 mm. The PCB boards were produced using a laminate with a T_g of 180 °C, which is almost 30–40 °C higher than the T_g of typical PCBs used for leaded soldering. As mentioned in Introduction, higher T_g is achieved by adding inorganic fillers to the PCB resin. This increases the PCB stiffness (hence stress levels) and facilitates PCB cracking. The stack-up of the board is given in Fig. 3. Inner layers included two signal layers and two ground layers.

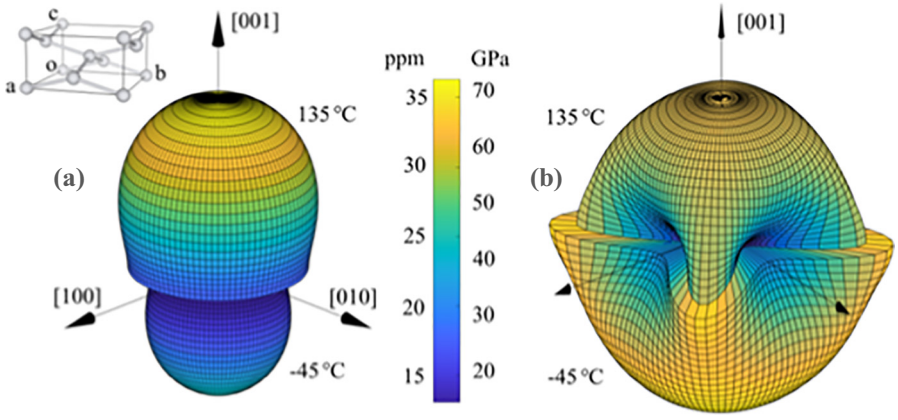

Fig. 1. Anisotropy and temperature-dependence of β-Sn properties. Distribution of a) coefficient of thermal expansion and b) elastic modulus of β-Sn at $-45\,^{\circ}C$ (graph bottom half) and $135\,^{\circ}C$ (graph top half). The values are in the Cartesian coordinate system for the tetragonal unit cell (top left insert) [25].

The surface finish on the PCB was electroless nickel/immersion gold (ENIG). Thermal cycling of the test vehicles was performed between $-40\,^{\circ}C$ and $100\,^{\circ}C$ with 10 min dwell time at the lower extreme and 30 min dwell time at the higher extreme. The temperature change rate was fixed at $10\,^{\circ}C$/min during both heating and cooling. Thus, a full thermal cycle took 68 min. The thermal cycling test was run for 6252 cycles. An event detector monitoring the daisy change resistance of the test patterns was used to record failures of the assemblies during thermal cycling.

In order to detect cracks in the PCB and solder joints induced during the thermal cycling test, cross-sections of thermally cycled resistors were studied. To this end, a high-speed diamond saw was used to cut out the samples. Zestron FA was then used to clean the cut-out samples and remove flux residues. In the next step, the samples were moulded in a room-temperature curing epoxy under low-vacuum. To facilitate detection of very small cracks in cross-sections of the samples, a fluorescent agent was dispensed into the moulding resin. Next, the moulded samples were cut out using the diamond blade to prepare samples. Successive grinding and polishing were performed to prepare the samples for further studies. An optical microscope with up to $\times 1000$ magnification was used to inspect the cross-sections of the prepared samples. Polarized light was used to determine the grain structure in the solder joints and UV light to detect cracks in the PCB laminate. Cross-sections of five as-soldered CR1206 components were inspected to determine typical grain structure in non-cycled solder joints and eventual cracking in the PCB laminate after soldering.

4. Finite element modelling

A finite element model was developed in ANSYS software to analyze the stress state in the PCB and predict damage evolution in the solder joints. The model was created using elements type Plane 183 under plane strain conditions. This assumption had negligible effect on the results, as the PCB stress and the solder creep strain changed less than 1% when plane stress conditions were assumed instead.

The stress state in the PCB in the immediate vicinity of the solder mask and the solder pad edges was calculated to assess the critical points of stress concentrations where damage can initiate in the PCB. In a structural finite element model, stresses at sharp corners between dissimilar materials are highly sensitive to the element size [32,33]. One possible solution to reduce mesh sensitivity is to round the sharp corners [33]. But the degree of rounding, i.e. the radius of curvature of the fillet in the sharp corners, has to be chosen arbitrarily, which may critically affect the stress results. Therefore, another solution was followed.

The primary aim of the finite element analysis is to compare the stress and damage parameters under various conditions (e.g. the grain orientation and PCB crack length) rather than their magnitude. Following the method proposed by Grant et al. [34], the stresses were hence extracted from a small distance from the sharp corners and interfaces to eliminate the effects of the singular points.

Fig. 4 shows a cross-section of a solder joint to a ceramic resistor and the corresponding finite element mesh. Linear-elastic material

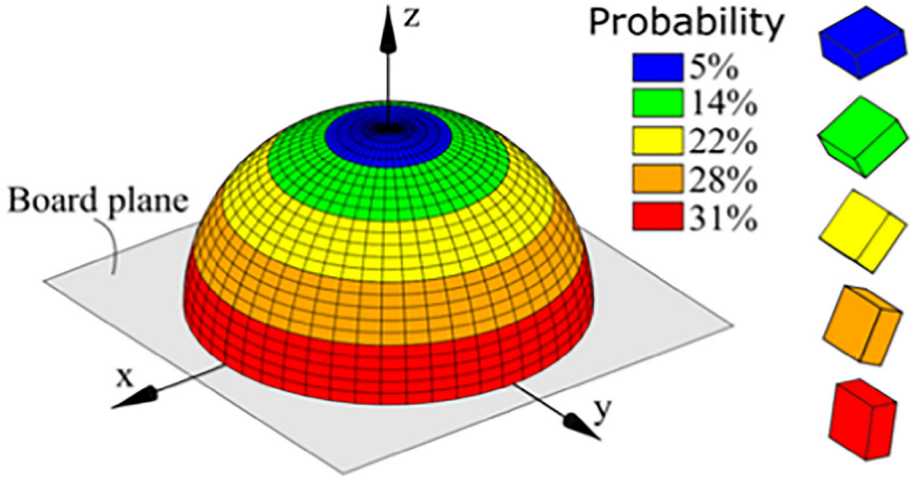

Fig. 2. The probability distribution of *c*-axis orientations. In a red joint, the *c*-axis is almost parallel to the board, while in a blue joint the *c*-axis is almost normal to the board [25]. (For interpretation of the references to colour in this figure, the reader is referred to the web version of this article.)

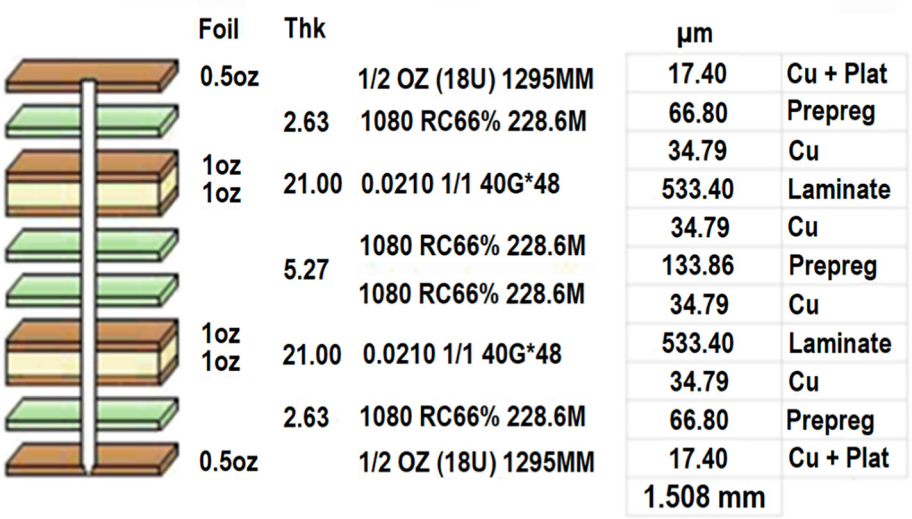

Fig. 3. Stack-up of the test board (solder mask not included).

models were used for the various constituents of the model (Table 1), except for the solder whose elastic behavior was simulated using an anisotropic model, because the solder joints were found to be mostly single-grained. Some studies obtain solder material properties from tensile tests performed on large specimens [35,36]. However, isotropic material models are not able to predict stress and strain states in single-grained joints with random orientation. Anisotropic elastic behavior of SnAgCu solder alloys highly depend on the solder composition and the degree of precipitation hardening caused by small tin-silver and tin-copper intermetallic particles in the solder. However, anisotropic elastic moduli and CTEs of these alloys are not available in the literature. Therefore, in this study anisotropic elastic properties and CTE of pure tin were used in the finite element simulations [25,37].

In addition, it has been shown that the creep behavior of the lead-free solder is a strong function of the grain orientation [38,39]. For simplicity, the creep anisotropy was ignored, and the solder creep behavior was simulated using an isotropic hyperbolic sine law:

$$\frac{d\varepsilon}{dt} = A[\sinh(\alpha\sigma)]^n \exp\left(\frac{-Q}{RT}\right) \quad (1)$$

where σ, R, and T denote the stress level, the universal gas constant, and the temperature, respectively. A, α, and n are the model constants and are determined from experimental characterization data [40]. The model parameters are reported in Table 2.

PCBs used for lead-free soldering consist of relatively brittle E-glass fibres and epoxy resin [19,41], and exhibit a nearly linear stress-strain relationship in uniaxial tensile tests [42]. Therefore, maximum first principal stress was used as the failure criterion to predict damage initiation location in the PCBs. Since the main objective of modelling PCB cracks was to provide a basis for relative comparison of different crack lengths, the PCB was modelled as a homogeneous material. Calculation of local values of PCB stresses requires a more detailed model including separate regions of resin and glass weaves and their respective properties.

Table 1
Properties of the resistor assembly. Coordinate y is normal to the plane of the PCB.

Material	Young's modulus (GPa)	Poisson's ratio	Thermal expansion coefficient (ppm/°C)
Copper pad	128	0.34	17
Solder mask	3	0.30	50
Resistor	320	0.30	6.8
PCB	$E_x = E_z = 17.9$ $E_y = 7.84$	$\upsilon_{xy} = \upsilon_{yz} = 0.39$ $\upsilon_{xz} = 0.11$	$\alpha_x = \alpha_z = 14.5$ $\alpha_y = 67.2$

Table 2
Parameters for solder creep model [38].

A	α (MPa)$^{-1}$	n	Q (kJ·K)	R (J/(K·mol))
6.07	0.68	2.3	55.8	8.314

5. Results and discussion

5.1. Experimental results

In this section, the experimental results of crack and damage initiation in the PCB and the solder joints are presented. Also, the

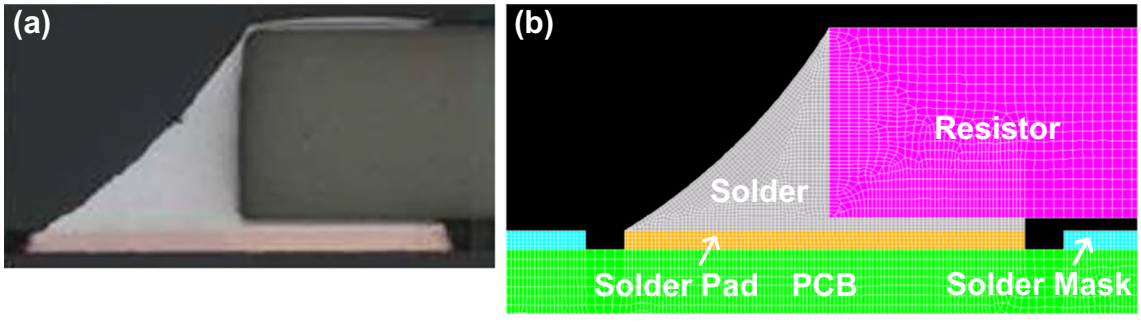

Fig. 4. a) Cross-section of the solder joint of the chip resistor. b) Corresponding finite element mesh.

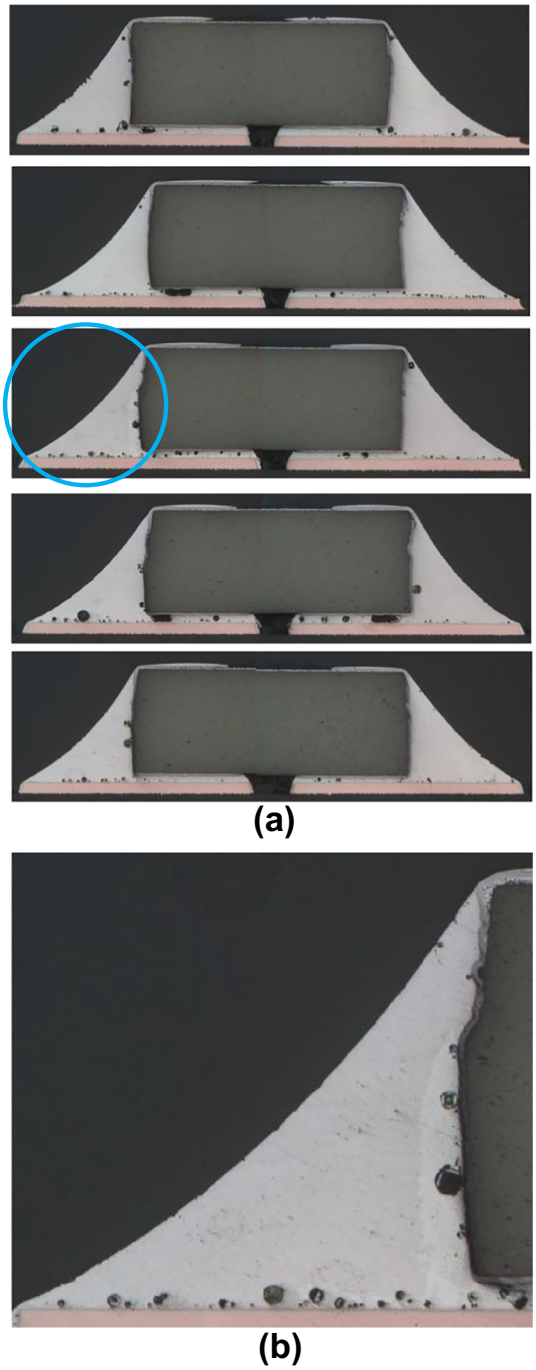

Fig. 5. a) Polarized light images of cross-sections of SAC305 solder joints to five CR1206. Out of the ten joints studied, nine were single-grained, and only one had CTG grain structure marked with a blue circle. b) Enlarged view of the solder joint with CTG structure. (For interpretation of the references to colour in this figure legend, the reader is referred to the web version of this article.)

predictions of the finite element simulations are presented in detail to explore the possible locations for crack initiation in the PCB and evaluate the effect of the solder grain orientation on the PCB stress distribution. The numerical results are discussed in terms of the experimental observations in Section 5.2.

Polarized light images of the cross-sections of the solder joints to the five as-soldered CR1206 components are shown in Fig. 5. Out of the ten solder joints investigated, nine appear to have single-grained structure and only one to have CTG structure. Since cross-sections only show the grain structure in the plane of the cross-sections, it is possible that some of the solder joints that seem to consist of only one grain may actually consist of more than one grain. Due to the randomness of the grain orientations, the two solder joints of each ceramic resistor shown in Fig. 5a possibly have different grain orientations. In addition, investigation of the cross-sections using UV light showed that no cracks had formed in the PCB laminate during reflow soldering.

After thermal cycling, cross-sectioning was performed for all five resistors from a test pattern that had failed after 5558 cycles. A complete crack through a solder joint was observed for one of the solder joints to all but one of the components. Cracks were also observed in the PCB close to the solder joints for all five resistors. The cracks propagated vertically into the surface resin layer, then deviated after they reached the glass weave. The average crack length was 10–40 μm. PCB cracks were found in all solder joints and always on the inner side of the solder joint under the component. Fig. 6 shows cross-sections of the solder joints to one of the resistors having typical cracks in the solder joints and PCB laminate. At nine of the solder joints, cracks were found close to the solder mask edge and at two of the solder joints, cracks were found close to the solder pad edge. That is, at one of the solder joints, cracks were observed both at the solder mask edge and at the solder pad edge (Fig. 7).

Since no cracks were observed in the PCB after soldering, the cracks must have formed during thermal cycling and not during soldering. The PCB cracks are assumed to form at the early stages of thermal cycling, therefore they can reduce stress in solder joint, and postpone solder cracking. If the cracks start to form in the PCB at the final stages of thermal cycling when creep damage has already been accumulated in the solder joint, PCB cracking will have a minor effect on solder fatigue life.

5.2. Finite element results

The first principal stress distribution in the PCB near the PCB-solder mask and PCB-solder pad interfaces was calculated using the finite element model. The critical points of stress concentration and crack initiation in the PCB, located on either side of each joint close to the solder mask and solder pad edges, are indicated in Fig. 8a. As explained in Section 4, for each pair of critical points the results were obtained one element away from the interface along the dashed lines shown in Fig. 8a to avoid stress singularities at sharp corners.

All solder joints were assumed to be single-grained. Various combinations of solder grain orientations were modelled to investigate its effect on the PCB stress state. The orientation of the *c*-axis of each of the two solder joints of the resistor is specified with two letters. The first letter indicates the joint location on either side of the component, while the second letter shows the grain orientation. For example, *Lx Ry* means the *c*-axes of left and right joints are parallel to *x* and *y* axes, respectively. In all cases the *c*-axis of the left joint was assumed to be parallel to the *x*-axis, while the *c*-axis of the right joint was taken to be parallel to either the *x*, *y* or *z* axis. Therefore, three different combinations of grain orientations were investigated: *Lx Rx*, *Lx Ry*, and *Lx Rz*. These combinations represent extreme cases of grain orientations, and therefore extreme cases of stress states, so that other possible combinations fall between theses extremes.

Fig. 8 shows distribution of the first principal stress in the PCB for various combinations of grain orientations. As expected, the stress is maximum near the sharp corners specified in Fig. 8a. Regardless of the solder grain orientation, the first principal stress is always larger on the inner side of the joints under the components. This is consistent with the experimental observations of PCB cracking on the inner side (Fig. 6).

Evaluating the effect of neighbouring solder joints' orientation on the PCB stress is made possible by comparing Fig. 8b and c. Although the orientation of the right solder joint has a negligible effect on the PCB stresses near the outer (left) side of left joint (Points A and B), it does affect the PCB stresses near the inner (right) side of left joint

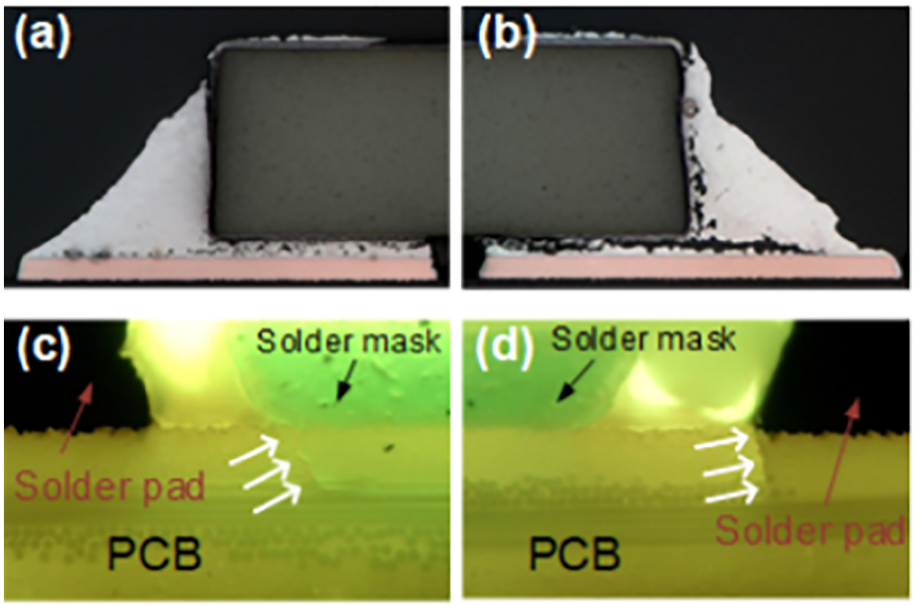

Fig. 6. Cross-sections of the solder joints to a thermally cycled resistor showing a–b) cracks in the two solder joints and c–d) cracks in the PCB laminate.

(Points C and D), simply because it is located at a closer distance to the right joint and is to a larger extent affected by its grain orientation.

Out of the three grain combinations considered, the *Lx Rx* case generates the highest stress in the PCB, because it maximizes the mismatch of thermomechanical properties in the *y* direction (perpendicular to board) between the component, the solder joint, and the board, hence increases the thermal stresses generated during thermal cycling. Also, since for this grain combination, the *c*-axis of both joints lies in *x*-direction, and the CTE and Young's modulus are both maximum along the *c*-axis, deformation of each joint is limited by the neighbouring joint.

In addition, the finite element simulations show that for the individual joints, the solder anisotropy influences the stress state in the PCB underneath the joint. In particular, the stress at outer points is highly affected by the grain orientation. For instance, in the *Lx Rx* case the stress at Point G is 126% higher than the *Lx Ry* combination. However, as mentioned above, the stress at inner points is always larger than at outer points, and PCB cracking always starts at the inner side of the joint under the component.

These observations show that the first principal stress is a reliable index to predict crack initiation in the PCBs under thermal loading and could be used as an effective tool to evaluate the effect of various geometrical and mechanical properties of the microelectronic assembly on PCB cracking.

It was also of interest to investigate the effect of the size and curvature of the solder joint fillet, which is controlled by parameters such as stencil thickness, on the stress state in the PCB. Fig. 9 depicts the effect of solder fillet curvature on the distribution of first principal stress in the PCB near the stress concentration points of the right joint for *Lx Rx* combination. Concave, straight, and convex fillets were modelled using the finite element analysis. It is observed that although the fillet curvature had a negligible effect on the stress distribution in the PCB on the inner (left) side of the joint (Points E and F in Fig. 9a), it significantly affected the stress at Point G. At this point, the convex fillet produced the highest stress with a maximum that was about 75% larger than that for concave fillet. In fact, it was even higher than for the stress levels at the inner points. Therefore, fillet curvature can possibly transfer the location of crack initiation from the joint inner side

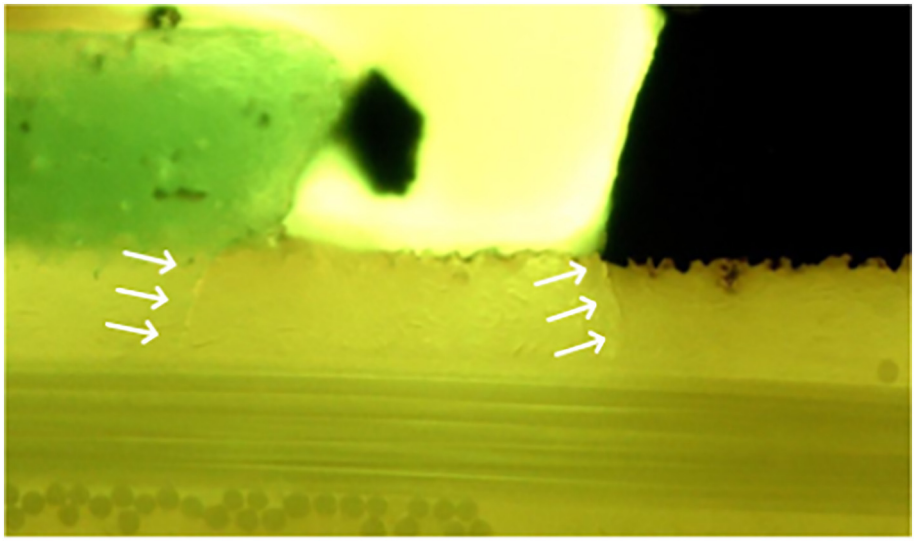

Fig. 7. Cross-sections of a solder joint to a thermally cycled resistor showing PCB cracks formed both at the PCB - solder mask edge and at the PCB - solder pad edge.

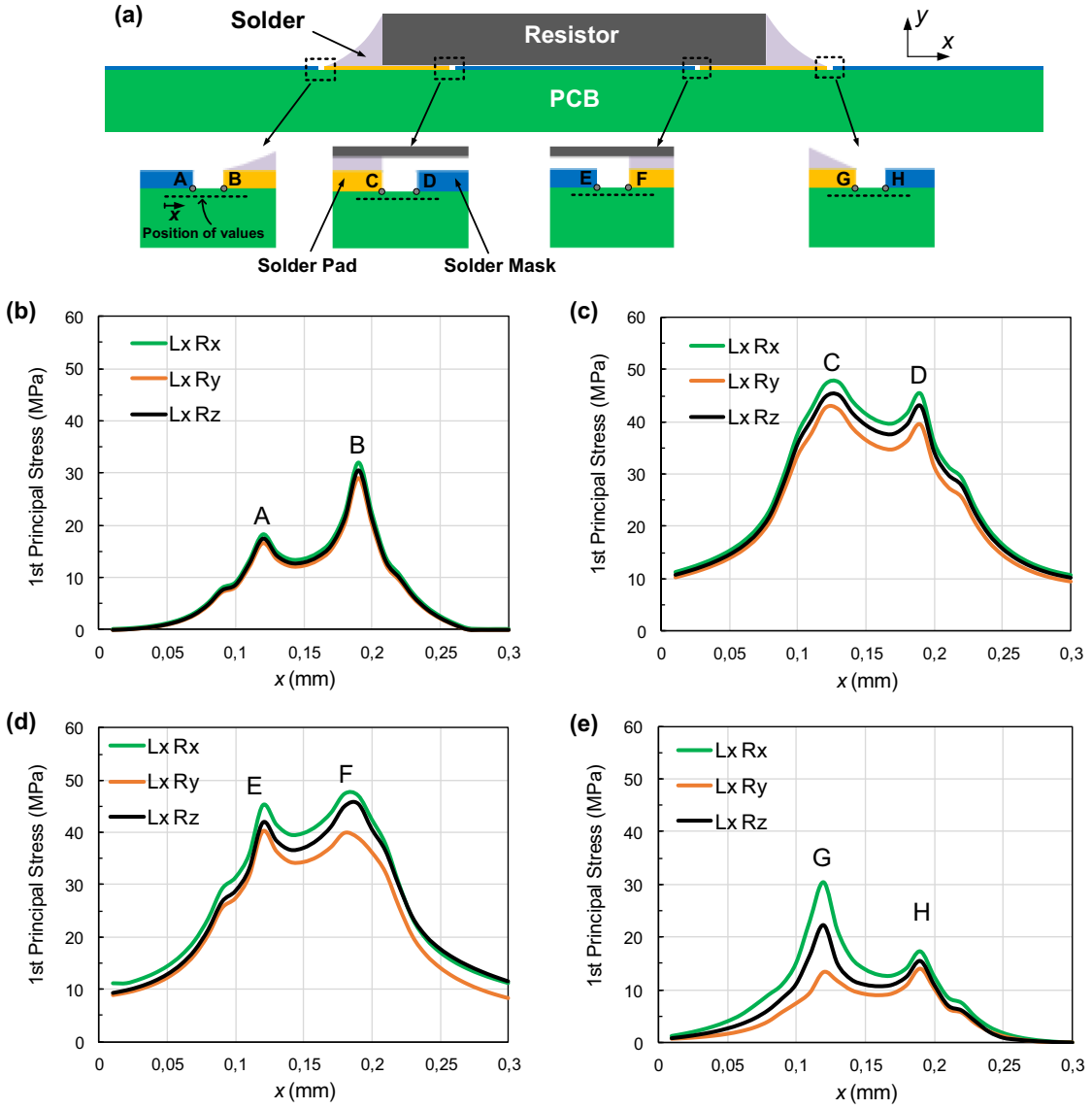

Fig. 8. Finite element results of the first principal stress distribution in the PCB at the vicinity of stress concentration points for a temperature change of −40 °C–100 °C. a) Schematic cross-section of resistor-solder-PCB assembly indicating eight critical points of stress concentration (Points A to H). Stresses are obtained along the dashed line specified near the stress concentration points on b) the outer (left) side of left joint (Points A and B), c) the inner (right) side of left joint (Points C and D), d) the inner (left) side of right joint (Points E and F), and e) the outer (right) side of right joint (Points G and H).

to the outer side. These trends show that the PCB stress near the region of the toe of the solder joint fillet is a strong function of the fillet curvature so that a concave fillet results in the minimum stress concentration.

Comparison of Figs. 8 and 9 shows that the PCB stress on the outer side of the solder joint is more influenced by the geometric and mechanical properties of the solder joints. On the inner side of the solder joint, under the component, the geometric constraint applied by the component and the neighbouring solder joint is the major factor dominating the PCB stress state.

In the next step, finite element analysis was used to study the creep damage in the solder joint and the effect of PCB cracking and solder grain orientation on damage parameters. Experimental cross-sectioning showed that cracking in the solder joint started near the component corner, then propagated in different directions (Fig. 10a). The creep deformation under thermal cycling is responsible for crack initiation in the solder joints [43–45]. Therefore, accumulated creep strain and creep work were calculated for a temperature change of −40 °C–100 °C using the finite element analysis to evaluate the critical points of damage initiation. Consistent with the experimental observations, the accumulated creep strain and creep work were both maximum near the component corner, as shown in Fig. 10b and c. Since solder cracking initiates close to the component corner (Fig. 10a), and damage parameters are maximum at this point (Fig. 10b and c), the values of accumulated creep strain and creep work were calculated near this point (Point O in Fig. 11a) along the dashed line. This enables quantitative comparisons of effects of grain orientation and PCB cracking.

Similar to Fig. 8, three combinations of grain orientations were modelled: *Lx Rx*, *Lx Ry*, and *Lx Rz*. Again, the *Lx Rx* grain combination generated the maximum value of damage in the solder at the vicinity of Point O. In the *Lx Rx* combination, the *c*-axis of both joints is along the *x*-axis, parallel to the board. This means the difference in thermo-mechanical properties is maximum in the *y*-direction. Moreover, with temperature change, each of the two solder joints tend to expand or contract maximally in *x*-direction, which is limited by the deformation of the neighbouring joint in the opposite direction. This is another reason the damage generated in the solder joint is maximum for the *Lx Rx* combination. Overall, the trends of accumulated creep strain and

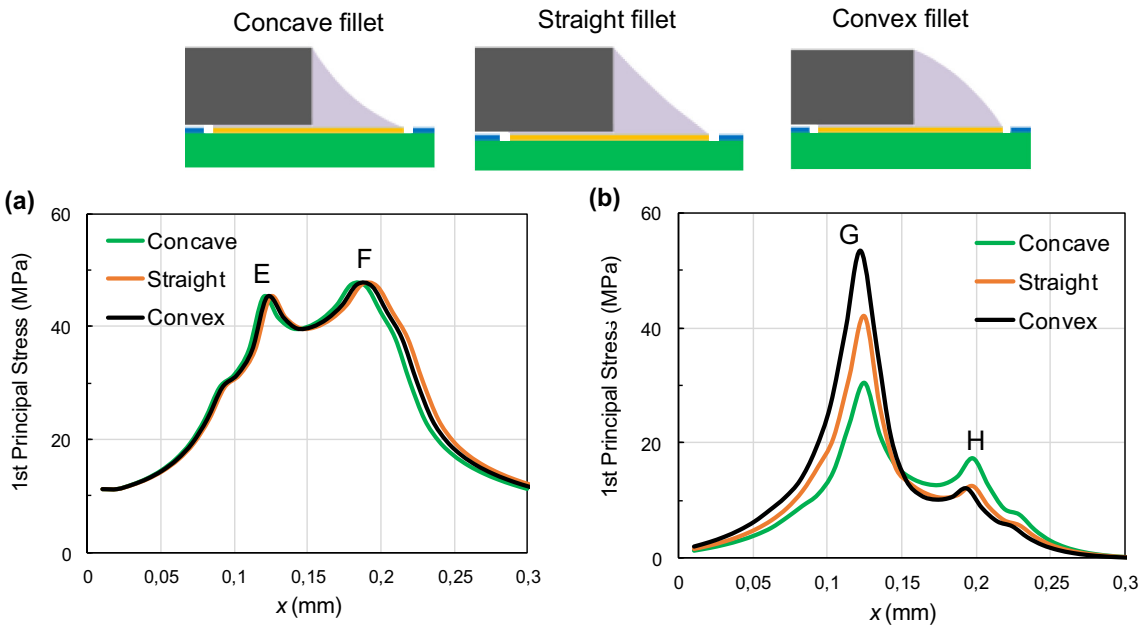

Fig. 9. Finite element results of the effect of solder fillet curvature on the first principal stress distribution in the PCB at the vicinity of the stress concentration points for *Lx Rx* grain combination. Stresses were calculated on a) the inner side (Points E and F), and b) outer side (Points G and H) of the right joint. The locations of these points are shown in Fig. 8a.

creep work are very similar, indicating either of these damage parameters can be used to evaluate damage and failure in the solder joints.

Evaluating the effect of PCB cracking on solder failure is of critical importance. For this purpose, cracks of various lengths were modelled in the PCB close to the PCB-solder pad edge, as shown in Fig. 12a. The crack length (CL in Fig. 12a) increased from 0.00 mm (the uncracked PCB) to 0.30 mm.

The accumulated creep strain and creep work were extracted along the dashed line in Fig. 12a. Both the creep strain and the creep work decrease with the increase of crack length in the PCB, because the presence of cracks in the PCB increase the PCB flexibility. For instance, the 0.100 mm long crack reduced the accumulated creep strain and creep work by 8% and 9%, respectively. This clearly shows that PCB cracking can alleviate damage in the solder and delay its failure. Since PCB cracking may be absent in field conditions, which are milder than testing conditions, life prediction based on accelerated testing conditions that cause PCB cracking can overestimate the life in field conditions.

In Fig. 12, PCB cracks of equal length were modelled on both sides of each joint. However, further simulations showed that the PCB cracks under the neighbouring joint have a negligible effect on the strain distribution and damage in the solder. Also, in Fig. 12 the PCB cracks were modelled near the PCB-solder pad edge. Modelling the PCB cracks near the PCB-solder mask edge changed the results by less than 3%.

A further question arises as to whether cracks on inner and outer sides of a specific joint have similar effects on damage reduction in that joint. In order to answer this question, four different cases were modelled, as shown in Fig. 13, which summarizes various crack location cases. The crack length was 0.10 mm in all cases. In Case 1 there was no crack in the PCB. In Case 2 and Case 3, a 0.10 mm long crack was modelled on the outer and inner sides of the joint, respectively. Finally, in Case 4 the crack was modelled on both sides. The results are shown in Fig. 13. It indicates, as expected, that the inner cracks have a greater impact on damage reduction in the solder joint. On the other hand, cracks on the outer side seem to have a negligible effect on solder damage.

Crack initiation and propagation in the PCB increases its compliance and flexibility locally near the solder joint, hence reduces damage in solder induced by thermal stresses. The PCB flexibility can also be decreased globally by using a thinner PCB. To show that the PCB cracking and the use of thinner PCBs have similar effects on strain reduction in the solder joints, several simulations were performed to compare the impact of these two parameters. The parameters varied in the model included the PCB thickness, and the crack length in the PCB. Fig. 14 shows that the accumulated creep strain and work in the 1.6 mm thick PCB with 50 μm and 100 μm long cracks were similar to those in the 1.2 mm and 0.8 mm thick PCB with no cracks, respectively. This further confirms the effect of PCB flexibility on damage in the solder joints.

6. Conclusions

Manufacturing processes of microelectronic assemblies have

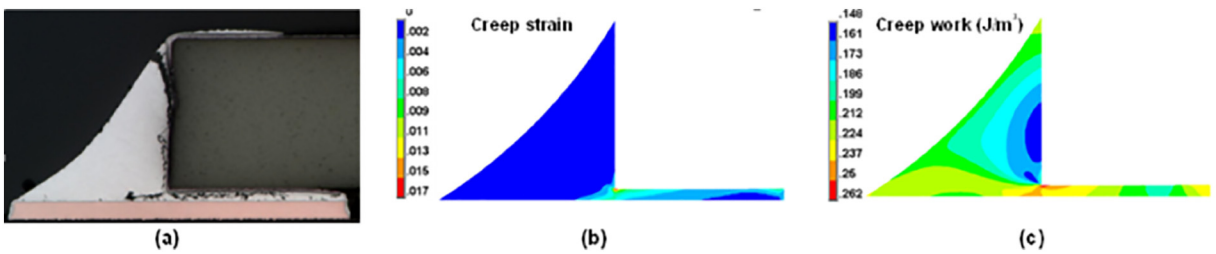

Fig. 10. a) Cross-section of a solder joint showing the crack propagation path under thermal cycling. Distribution of b) accumulated creep strain, and c) creep work in the solder joint.

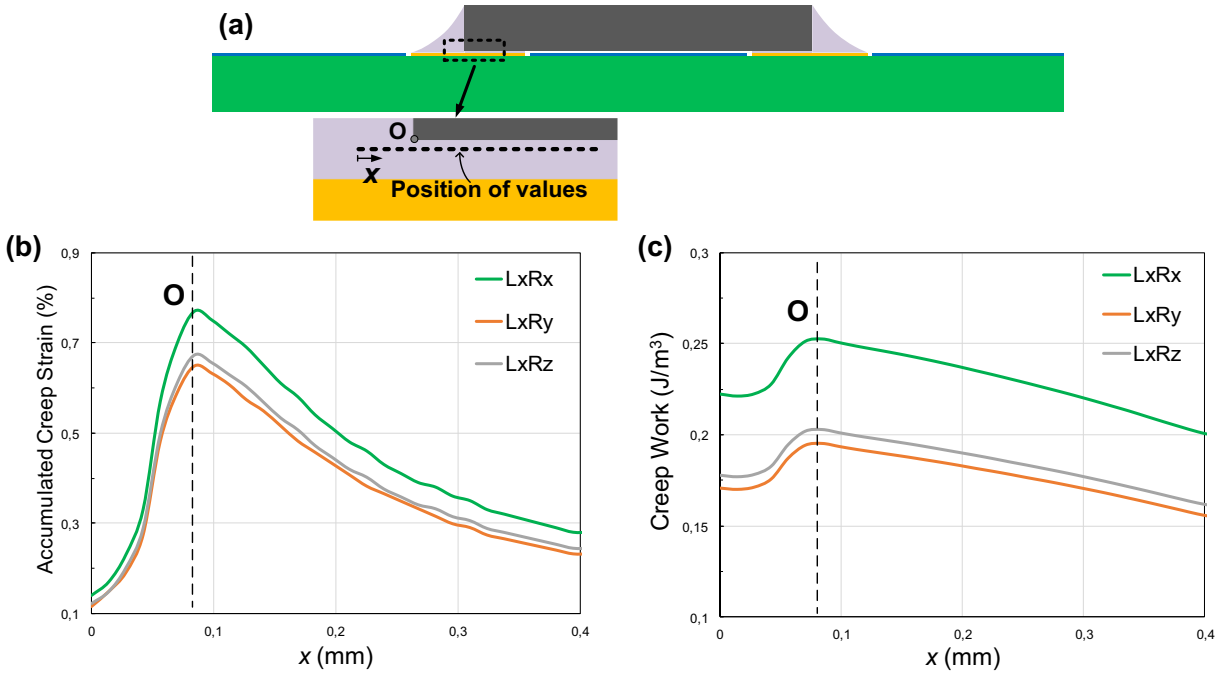

Fig. 11. Finite element results of the accumulated creep strain and creep work distribution in the left solder joint at the vicinity of component corner. a) Schematic view of resistor-solder-PCB assembly. The values of b) accumulated creep strain and c) creep work were extracted near Point O one element away from the solder-component interface, along the dashed line, for three different combinations of solder grain orientations.

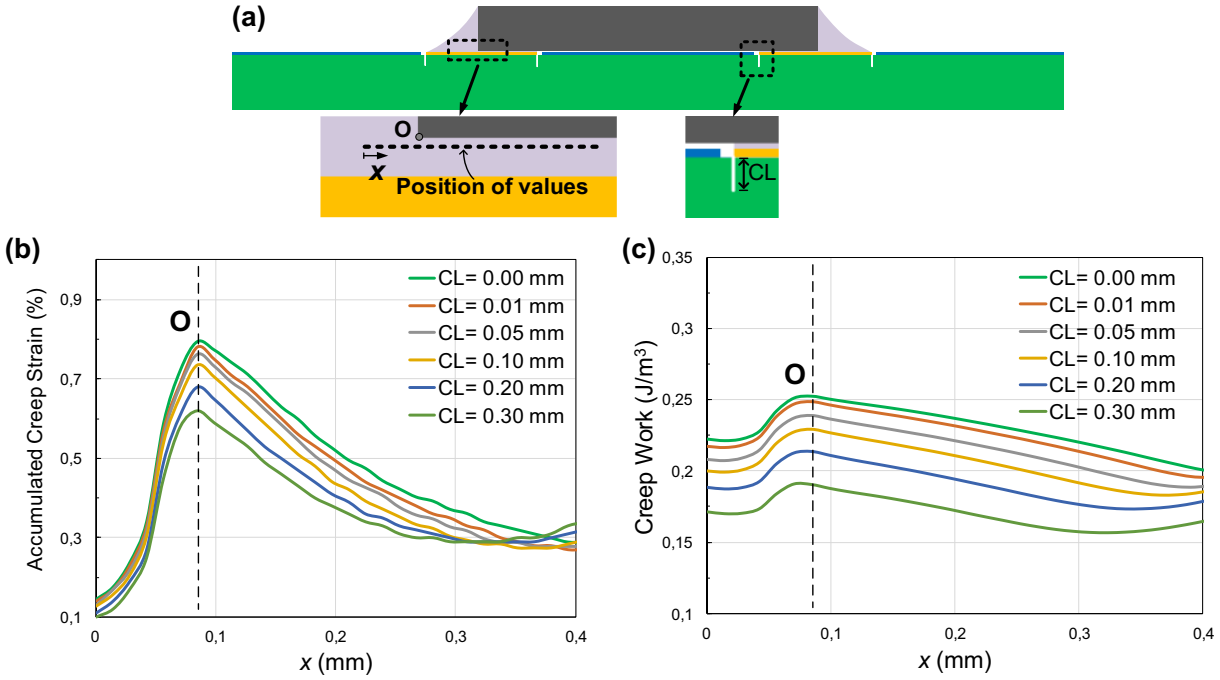

Fig. 12. Effect of crack length in the PCB on the creep strain and creep work in the left solder joint. Cracks of similar length were modelled on both sides of each joint, near the PCB-solder pad interface. a) Schematic view of the assembly cross-section indicating crack modelled in the PCB. Damage parameters were extracted at the vicinity of the component corner (Point O), one element away from the solder-component interface, along the dashed line. Effects of PCB crack length on a) the accumulated creep strain and b) creep work distribution in the solder joint.

significantly changed over the past twenty years. In particular, lead-free soldering using tin-based alloys has introduced new reliability challenges. Tin-based solder joints are often single-grained and exhibit highly anisotropic properties. Random orientation of the grain structure induces unique stress and strain state in each solder joint as well as in the PCB laminate. Formation of PCB cracks under single-grained solder joints is one of the issues that may have unexpected consequences on the solder joint reliability.

In this study, CR1206 components were assembled on FR4 laminate using SAC305 solder paste. After thermal cycling, PCB cracks were observed under solder pads of the components. Since no cracks were observed in the PCB laminate after soldering, they must have formed during the thermal cycling. Such cracks can reduce the thermo-mechanical stress on the solder joints during thermal cycling, resulting in

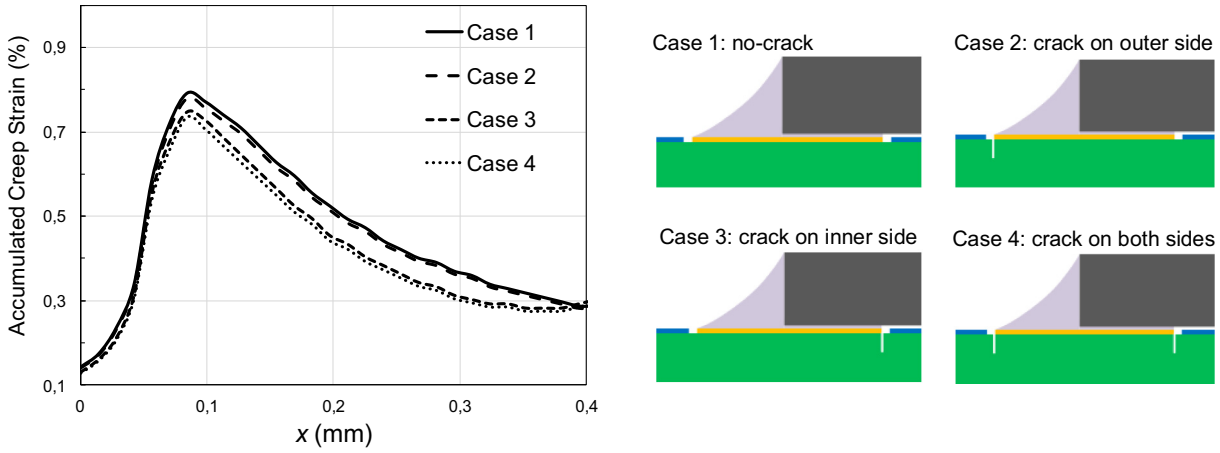

Fig. 13. Effect of the location of the PCB cracks on the accumulated creep strain distribution in the solder joint. A 0.10 mm long crack was modelled in various locations in the PCB. Creep strain values were extracted one element away from the solder-component interface, along the dashed line shown in Fig. 12a.

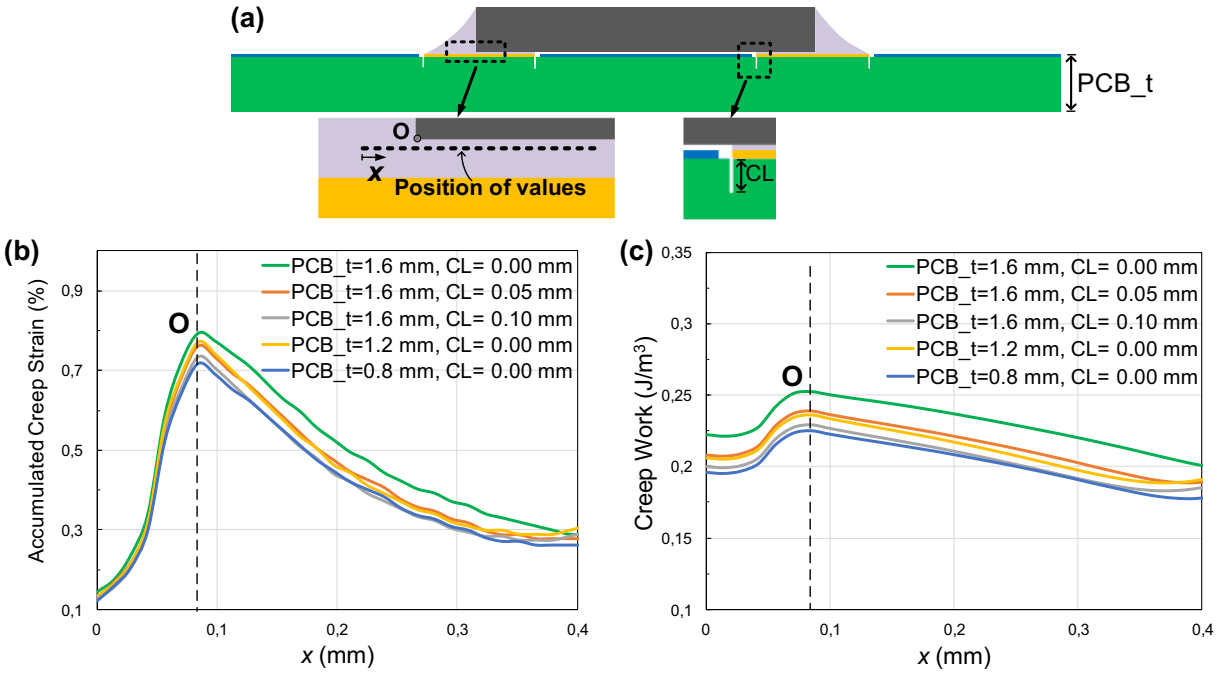

Fig. 14. Comparison of the effects of crack length in PCB and the PCB thickness on the creep strain reduction in the solder joint. a) Accumulated creep strain and b) creep work distribution in the solder joint were extracted one element away from the solder-component interface, along the dashed line.

an overestimation of the fatigue life of the solder joints in field conditions.

A creep model was coupled with a finite element analysis to simulate damage evolution in the solder joints influenced by PCB cracking. Modelling was performed for several grain orientation combinations. The modelling results show that the sharp corners at the edges of PCB-solder mask and PCB-solder pad interfaces generate stress concentration points, and are potential sites for crack initiation in the PCB.

In addition, cracks of various lengths were modelled in the PCB. The model was able to predict the location of damage initiation in the solder and PCB. It also confirmed that the presence of cracks in the PCB increased the PCB compliance and decreased the maximum accumulated creep strain and creep work in the solder joint. The effect of PCB crack length and solder fillet curvature was also studied. The modelling results were in good agreement with the experimental data, confirming the effectiveness of this approach for examining damage initiation in solder joints. In this study, the PCB was modelled as a homogeneous material for relative comparison of stress levels. However, it is heterogeneous because it has at least two phases (resin and glass fibre weave) with different properties. Accurate calculation of the PCB stress requires a more detailed model incorporating distribution of fibres and resin based on their specific material properties. The heterogeneous model would also allow to simulate crack propagation at the interface of fibre and resin after the crack reaches the fibre weave.

Acknowledgement

This work has been conducted within the Swedish national project "Requirements, specification and verification of environmental protection and life of solder joints to components" supported by the Swedish Governmental Agency for Innovation Systems (Vinnova) under contract 2015-01420.

References

[1] C. Barbagallo, G. Malgioglio, G. Petrone, G. Cammarata, Thermal fatigue life

evaluation of SnAgCu solder joints in a multi-chip power module, J. Phys. Conf. Ser. 841 (2017) 012014–012020 (IOP Publishing).
[2] L. Benabou, V. Etgens, Q.B. Tao, Finite element analysis of the effect of process-induced voids on the fatigue lifetime of a lead-free solder joint under thermal cycling, Microelectron. Reliab. 65 (2016) 243–254.
[3] P. Borgesen, L. Wentlent, S. Khasawneh, S. Shirazi, D. Schmitz, T. Alghoul, C. Greene, L. Yin, A mechanistic thermal fatigue model for SnAgCu solder joints, J. Electron. Mater. 47 (2018) 2526–2544.
[4] J. Chen, Y. Yin, J. Ye, Y. Wu, Investigation on fatigue behavior of single SnAgCu/SnPb solder joint by rapid thermal cycling, Solder. Surf. Mt. Technol. 27 (2015) 76–83.
[5] R.J. Coyle, K. Sweatman, B. Arfaei, Thermal fatigue evaluation of Pb-free solder joints: results, lessons learned, and future trends, JOM 67 (2015) 2394–2415.
[6] E. Dalton, G. Ren, J. Punch, M.N. Collins, Accelerated temperature cycling induced strain and failure behaviour for BGA assemblies of third generation high Ag content Pb-free solder alloys, Mater. Des. 154 (2018) 184–191.
[7] S. Shirazi, L. Yin, S. Khasawneh, L. Wentlent, P. Borgesen, Effects of solder joint dimensions and assembly process on acceleration factors and life in thermal cycling of SnAgCu solder joints, Electronic Components and Technology Conference (ECTC), 2015 IEEE 65th, IEEE, 2015.
[8] Q. Zhou, B. Zhou, T.-K. Lee, T. Bieler, Microstructural evolution of SAC305 solder joints in wafer level chip-scale packaging (WLCSP) with continuous and interrupted accelerated thermal cycling, J. Electron. Mater. 45 (2016) 3013–3024.
[9] M.M. Basit, M. Motalab, J.C. Suhling, Z. Hai, J. Evans, M.J. Bozack, P. Lall, Thermal cycling reliability of aged PBGA assemblies-comparison of Weibull failure data and finite element model predictions, Electronic Components and Technology Conference (ECTC), 2015 IEEE 65th, IEEE, 2015.
[10] G. Elger, S.V. Kandaswamy, E. Liu, A. Hanss, M. Schmid, R. Derix, F. Conti, Analysis of solder joint reliability of high power LEDs by transient thermal testing and transient finite element simulations, Microelectron. J. 46 (2015) 1230–1238.
[11] B. Gao, F. Yang, M. Chen, Y. Chen, W. Lai, C. Liu, Thermal lifetime estimation method of IGBT module considering solder fatigue damage feedback loop, Microelectron. Reliab. 82 (2018) 51–61.
[12] T.R. Bieler, B. Zhou, L. Blair, A. Zamiri, P. Darbandi, F. Pourboghrat, T.-K. Lee, K.-C. Liu, The role of elastic and plastic anisotropy of Sn in recrystallization and damage evolution during thermal cycling in SAC305 solder joints, J. Electron. Mater. 41 (2012) 283–301.
[13] P.-E. Tegehall, G. Wetter, Impact of laminate cracks under solder pads on the fatigue lives of ball grid array solder joints, Microelectron. Reliab. 55 (2015) 2354–2370.
[14] Z. Ma, S. Belyakov, K. Sweatman, T. Nishimura, C. Gourlay, Harnessing heterogeneous nucleation to control tin orientations in electronic interconnections, Nat. Commun. 8 (2017) 1916.
[15] C. Gourlay, S. Belyakov, Z. Ma, J. Xian, Nucleation and growth of tin in Pb-free solder joints, JOM 67 (2015) 2383–2393.
[16] J. Xian, Z. Ma, S. Belyakov, M. Ollivier, C. Gourlay, Nucleation of tin on the Cu6Sn5 layer in electronic interconnections, Acta Mater. 123 (2017) 404–415.
[17] T.R. Bieler, H. Jiang, L.P. Lehman, T. Kirkpatrick, E.J. Cotts, B. Nandagopal, Influence of Sn grain size and orientation on the thermomechanical response and reliability of Pb-free solder joints, IEEE Trans. Compon. Packag. Technol. 31 (2008) 370–381.
[18] B. Sood, R. Sanapala, D. Das, M. Pecht, C. Huang, M. Tsai, Comparison of printed circuit board property variations in response to simulated lead-free soldering, IEEE Trans. Electron. Packag. Manuf. 33 (2010) 98–111.
[19] C.F. Coombs, Printed Circuits Handbook, McGraw-Hill, New York, 2016.
[20] D. Xie, D. Shangguan, H. Kroener, Pad cratering evaluation of PCB, Proc IPC APEX EXPO, 2006.
[21] G. Long, T. Embree, M. Mukadam, S. Parupalli, V. Vasudevan, Lead free assembly impacts on laminate material properties and “pad crater” failures, Proc IPC APEX EXPO, 2007.
[22] V. Raghavan, B. Roggeman, M. Meilunas, P. Borgesen, Effects of pre-stressing on solder joint failure by pad cratering, Proc Electronics Components Technology Conference, 2010, pp. 456–463.
[23] V. Raghavan, B. Roggeman, M. Meilunas, P. Borgesen, Effects of ‘Latent Damage’ on pad cratering: reduction in life and a potential change in failure mode, Microelectron. Reliab. 53 (2013) 303–313.
[24] L.F. Da Silva, R. Adams, Techniques to reduce the peel stresses in adhesive joints with composites, Int. J. Adhes. Adhes. 27 (2007) 227–235.
[25] A. Lövberg, P.-E. Tegehall, S. Akbari, D. Andersson, On the formation and propagation of laminate cracks and their influence on the fatigue lives of solder joints, Thermal, Mechanical and Multi-physics Simulation and Experiments in Microelectronics and Microsystems (EuroSimE), 2018 19th International Conference on, IEEE, 2018.
[26] J. Hagberg, J. Putaala, J. Raumanni, O. Salmela, T. Galkin, BGA interconnection reliability in mirrored module configurations, IEEE Trans. Compon. Packag. Manuf. Technol. 7 (2017) 1634–1643.
[27] J. Xian, G. Zeng, S. Belyakov, Q. Gu, K. Nogita, C. Gourlay, Anisotropic thermal expansion of Ni3Sn4, Ag3Sn, Cu3Sn, Cu6Sn5 and βSn, Intermetallics 91 (2017) 50–64.
[28] A. Lövberg, P.-E. Tegehall, G. Wetter, K. Brinkfeldt, D. Andersson, Simulations of the impact of single-grained lead-free solder joints on the reliability of ball Grid Array components, Thermal, Mechanical and Multi-physics Simulation and Experiments in Microelectronics and Microsystems (EuroSimE), 2017 18th International Conference on, IEEE, 2017.
[29] B. Arfaei, M. Anselm, F. Mutuku, E. Cotts, AREA-effect of PCB Surface Finish on Sn Grain Morphology and Thermal Fatigue Performance of Lead-free Solder Joints, SMTA International, 2014.
[30] P. Darbandi, T.R. Bieler, F. Pourboghrat, T.-k. Lee, The effect of cooling rate on grain orientation and misorientation microstructure of SAC105 solder joints before and after impact drop tests, J. Electron. Mater. 43 (2014) 2521–2529.
[31] T.-K. Lee, K.-C. Liu, T.R. Bieler, Microstructure and orientation evolution of the Sn phase as a function of position in ball grid arrays in Sn-Ag-Cu solder joints, J. Electron. Mater. 38 (2009) 2685.
[32] R. Adams, R. Atkins, J. Harris, A. Kinloch, Stress analysis and failure properties of carbon-fibre-reinforced-plastic/steel double-lap joints, J. Adhes. 20 (1986) 29–53.
[33] R. Adams, J. Harris, The influence of local geometry on the strength of adhesive joints, Int. J. Adhes. Adhes. 7 (1987) 69–80.
[34] L. Grant, R. Adams, L.F. da Silva, Experimental and numerical analysis of single-lap joints for the automotive industry, Int. J. Adhes. Adhes. 29 (2009) 405–413.
[35] F. Che, W. Zhu, E.S. Poh, X. Zhang, X. Zhang, The study of mechanical properties of Sn–Ag–Cu lead-free solders with different Ag contents and Ni doping under different strain rates and temperatures, J. Alloys Compd. 507 (2010) 215–224.
[36] P. Lall, S. Shantaram, D. Locker, High strain rate properties of SAC105 and SAC305 leadfree alloys after extended high temperature storage, J. SMTA 27 (2014) 13–27.
[37] S. Park, R. Dhakal, J. Gao, Three-dimensional finite element analysis of multiple-grained lead-free solder interconnects, J. Electron. Mater. 37 (2008) 1139–1147.
[38] S. Mukherjee, B. Zhou, A. Dasgupta, T.R. Bieler, Mechanistic modeling of the anisotropic steady state creep response of SnAgCu SINGLE Crystal, ASME 2015 International Technical Conference and Exhibition on Packaging and Integration of Electronic and Photonic Microsystems collocated with the ASME 2015 13th International Conference on Nanochannels, Microchannels, and Minichannels, American Society of Mechanical Engineers, 2015.
[39] S. Mukherjee, B. Zhou, A. Dasgupta, T.R. Bieler, Multiscale modeling of the anisotropic transient creep response of heterogeneous single crystal SnAgCu solder, Int. J. Plast. 78 (2016) 1–25.
[40] G. Cuddalorepatta, M. Williams, A. Dasgupta, Viscoplastic creep response and microstructure of As-fabricated microscale Sn-3.0 Ag-0.5 Cu solder interconnects, J. Electron. Mater. 39 (2010) 2292–2309.
[41] H. Li, Alumina and silica sources for E-glass fibre manufacturing–melting energy aspects, Glass Technol.: Eur. J. Glass Sci. Technol., Part A 55 (2014) 7–13.
[42] S. Akbari, A. Nourani, J.K. Spelt, Effect of adhesive fillet geometry on bond strength between microelectronic components and composite circuit boards, Compos. A: Appl. Sci. Manuf. 87 (2016) 228–236.
[43] N. Fu, J.C. Suhling, P. Lall, Evolution of the cyclic stress-strain and constitutive behaviors of SAC305 lead free solder during fatigue testing, Thermal and Thermomechanical Phenomena in Electronic Systems (ITherm), 2017 16th IEEE Intersociety Conference on, IEEE, 2017.
[44] M. Hasnine, J.C. Suhling, M.J. Bozack, Effects of high temperature aging on the microstructural evolution and mechanical behavior of SAC305 solder joints using synchrotron X-ray microdiffraction and nanoindentation, J. Mater. Sci. Mater. Electron. 28 (2017) 13496–13506.
[45] M. Serebreni, R. Wilcoxon, D. Hillman, N. Blattau, C. Hillman, The effect of improper conformal coating on SnPb and Pb-free BGA solder joints during thermal cycling: experiments and modeling, Thermal Measurement, Modeling & Management Symposium (SEMI-THERM), 2017 33rd, IEEE, 2017.